This is a repository copy of *A tissue-engineered model of T-cell–mediated oral mucosal inflammatory disease*.

White Rose Research Online URL for this paper:
https://eprints.whiterose.ac.uk/222289/

Version: Published Version

Article:

El-Howati, A. orcid.org/0000-0002-4263-6846, Edmans, J.G. orcid.org/0000-0002-4539-9145, Santocildes-Romero, M.E. orcid.org/0000-0003-3805-3055 et al. (3 more authors)

A Tissue-Engineered Model of T-Cell−Mediated Oral Mucosal Inflammatory Disease

Asma El-Howati[1,2], Jake G. Edmans[1,3], Martin E. Santocildes-Romero[4], Lars Siim Madsen[4], Craig Murdoch[1,5] and Helen E. Colley[1,5]

T-cell−mediated oral mucocutaneous inflammatory conditions, including oral lichen planus, are common, but development of new treatments aimed at relieving symptoms and controlling oral lichen planus progression is hampered by the lack of experimental models. In this study, we developed a tissue-engineered oral mucosal equivalent containing polarized T-cells to replicate oral lichen planus pathogenesis. Peripheral blood CD4+ and CD8+ T-cells were isolated, activated, and polarized into T helper 1 and cytotoxic T cells. Oral mucosal equivalents were constructed by culturing oral keratinocytes on an oral fibroblast−populated hydrogel to produce a stratified squamous epithelium. Oral mucosal equivalent stimulated with IFN-γ and TNF-α or medium from T helper 1 cells caused increased secretion of inflammatory cytokines and chemokines. A model of T-cell−mediated inflammatory disease was developed by combining oral mucosal equivalent on top of a T helper 1 and cytotoxic T-cell−containing hydrogel, followed by epithelial stimulation with IFN-γ and TNF-α. T-cell recruitment toward the epithelium was associated with increased secretion of T-cell chemoattractants CCL5, CXCL9, and CXCL10. Histological assessment showed tissue damage associated with cleaved caspase-3 and altered laminin-5 expression. Treatment with inhibitors directed against Jak, $K_{Ca}3.1$ channels, or clobetasol in solution and through a mucoadhesive patch prevented cytokine and chemokine release and tissue damage. This disease model has potential to probe for mechanisms of pathogenesis or as a test platform for novel therapeutics or treatment modalities.

Keywords: Drug delivery, Oral lichen planus, Oral medicine, Tissue engineering

INTRODUCTION

T-cell−mediated inflammatory diseases of the oral mucosa such as oral lichen planus (OLP) are common, affecting up to 1.7% of the global population (González-Moles et al, 2021). OLP, a disease of unknown etiology, classically presents with reticular white lesions that are bilaterally and symmetrically distributed on the oral mucosa. Thickening of the oral mucosa may be relatively asymptomatic, but with increasing disease severity, there is mucosal thinning leading to the generation of erosive (atrophic) lesions that often present as painful ulcers (Carrozzo et al, 2019). The histopathological features of OLP include a dense subepithelial band of inflammatory T-cells, along with intraepithelial T-cell infiltration, apoptosis of basal cells in the stratum basale, and

liquefaction of the basement membrane (Matthews et al, 1984).

OLP pathogenesis is initially driven by the recognition of nonself-antigen(s) by Langerhans cells within the oral mucosa, leading to secretion of proinflammatory cytokines (predominantly IFN-γ and TNF-α) that evoke a complex interplay between immune and nonimmune cells, increased production of cytokines, increased cell surface expression of adhesion molecules, and increased secretion of T-cell−recruiting chemokines (reviewed in El-Howati et al [2023]). These events lead to significant infiltration of T-cells at lesional sites and culminate in a dysregulated T-cell−mediated immune reaction that drive keratinocyte apoptosis and proteolytic-mediated basement membrane proteolysis (DeAngelis et al, 2019; Matthews et al, 1984). Previous studies suggest that the cytokine milieu in OLP skews CD4+ T-cell polarization mainly toward a T helper 1 (Th1) phenotype that then drives the activation of cytotoxic CD8+ T-cells, although evidence suggest that other T helper cell types (T helper 17, T helper 9) may also be involved (El-Howati et al, 2023). Treatment is usually through the use of topical or systemic corticosteroids, although there is no consensus treatment for OLP, and investigations into the pathogenic mechanisms or development of novel therapeutics are hampered by the lack of experimental models.

Significant advances have been made in the development of tissue-engineered oral mucosal equivalents (OMEs) (Colley et al, 2011; Jennings et al, 2016; Klausner et al, 2021), but

[1]School of Clinical Dentistry, University of Sheffield, Sheffield, United Kingdom; [2]Department of Oral Medicine, Faculty of Dentistry, University of Benghazi, Benghazi, Libya; [3]Department of Chemistry, University of Sheffield, Sheffield, United Kingdom; [4]AFYX Therapeutics, Hørsholm, Denmark; and [5]Insigneo Institute, University of Sheffield, Sheffield, United Kingdom

Correspondence: Craig Murdoch, School of Clinical Dentistry, University of Sheffield, 19 Claremont Crescent, Sheffield S10 2TA, United Kingdom. E-mail: c.murdoch@sheffield.ac.uk

relatively, few studies have reported the incorporation of immune cells into these models, where only monocytes and macrophages have been added (Bao et al, 2015; Björnfot Holmström et al, 2017; Lira-Junior et al, 2020; Ollington et al, 2021; Xiao et al, 2018). Although there are reports of addition of T-cells (Engelhart et al, 2005), T helper cell subsets (van den Bogaard et al, 2014), or exogenous T-cell cytokines (ie, recombinant IL-4 and IL-13) to tissue-engineered skin equivalents to produce in vitro models that resemble atopic dermatitis or psoriasis (Danso et al, 2014; Jang et al, 2023; Lorthois et al, 2019), to date, no studies have reported the addition of T-cells to OMEs in an attempt to replicate T-cell−mediated oral disease.

In this study, we describe the generation of a tissue-engineered inflammatory model of the oral mucosa that contains primary activated and Th1-polarized human CD4+ and CD8+ cytotoxic T (Tc) cells. These T-cell−containing OMEs produced inflammatory responses in the form of increased secretion of proinflammatory cytokines, chemokines, T-cell recruitment, and tissue damage that replicate those observed in vivo. Furthermore, upon application with either Jak inhibitor, a $K_{Ca}3.1$ channel inhibitor, or corticosteroid applied topically as a solution or through a drug-containing mucoadhesive electrospun patch, disease parameters were significantly reduced. These inflammatory OMEs will be extremely beneficial for studies aimed at dissecting the molecular mechanism of disease pathogenesis or to test novel treatment strategies.

RESULTS

Primary T-cell isolation, activation, and polarization for incorporation into a 3-dimensional collagen hydrogel

CD4+ and CD8+ T-cells were isolated from blood with high purity (91.7 ± 3.5% and 92.6 ± 3.0%, respectively) and viability (>87.5%) (Supplementary Figure S1a and b). T-cell activation using CD3 and CD28 ligation for 24 hours was evidenced by increased CD69 cell surface abundance compared with that of untreated controls ($P = .03$) (Supplementary Figure S1c). After IL-12, IL-18, and anti−IL-4 treatment, polarization of CD4+ T-cells to a Th1 phenotype was confirmed by significantly increased gene expression ($P < .01$) (Supplementary Figure S1d) and nuclear abundance ($P < .05$) (Figure 1a) of T-bet transcription factor, along with the transcription factor signal transducer and activator of transcription 4 (Supplementary Figure S1d), both key regulators of the Th1 phenotype (El-Howati et al, 2023), as well as increased secretion of IFN-γ ($P < .01$) (Figure 1b) compared with that of both naïve and CD3 and CD28 activated T-cells. Secretion of TNF-α was increased compared with that in naïve but not in activated T-cells ($P < .05$) (Figure 1c). Although Th1 cells displayed a lower rate of expansion than CD3 and CD28 activated cells, they showed an exponential growth rate after day 3, with levels 3-fold greater than those of naïve T-cell proliferation by day 7 ($P < .05$) (Figure 1d).

After activation, naïve CD8+ T cells were converted to Tc cells upon stimulation with IL-2 and CD3 and CD28 ligation in the presence of CD4+ T-cells. These cells displayed
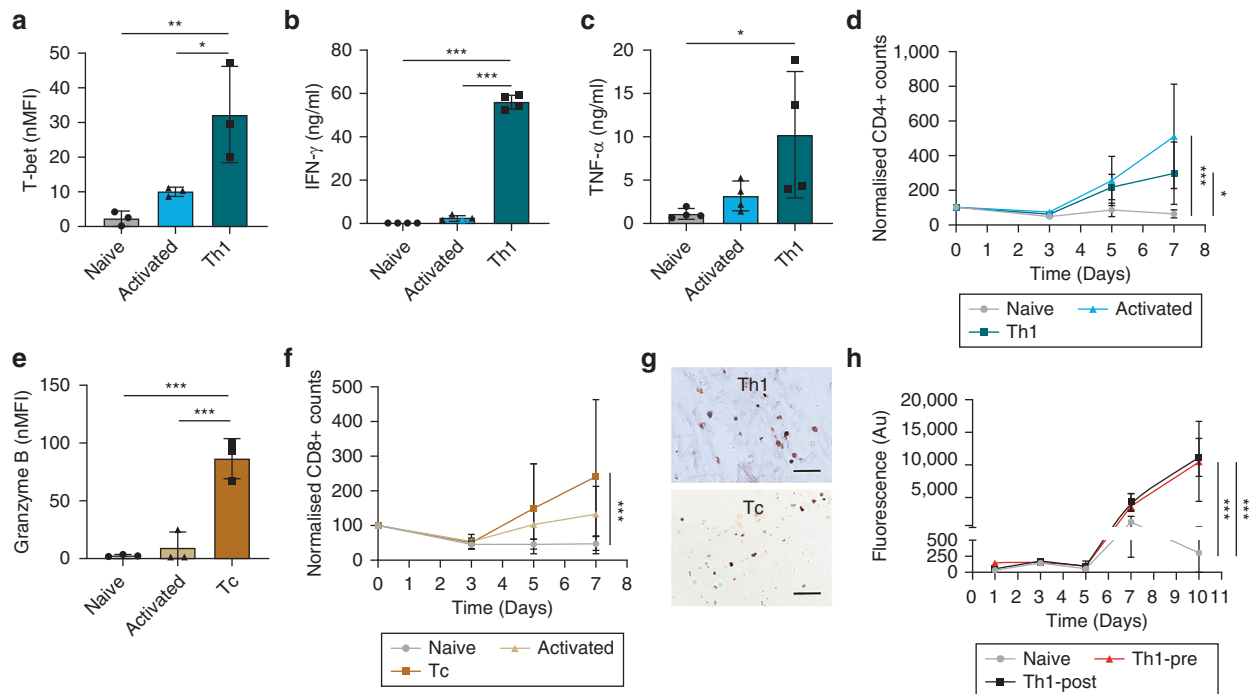

Figure 1. Phenotyping Th1 and CD8+ T-cell activation in monolayer and 3D hydrogels. CD4+ T-cells were treated with IL-2, IL-2, and CD3 and CD28 or Th1-differentiation media for 7 days and referred to as naïve, activated, or Th1, respectively. **(a−c)** Abundance of T-bet by **(a)** flow cytometry and secretion of inflammatory cytokines **(b)** IFN-γ and **(c)** TNF-α by ELISA. **(d)** CD4+ T-cell proliferation over 7 days assessed by cell counting. CD8+ T-cells were treated with IL-2, IL-2, and CD3 and CD28 or CD3 and CD28 in the presence of CD4+ T cells for 7 days and referred to as naïve, activated, or CD8+ Tc cells, respectively. **(e)** Presence of granzyme B by flow cytometry, **(f)** differences in CD8+ T-cell number over 7 days by cell counting, **(g)** morphology of CD4+ and CD 8+ T-cells in a collagen hydrogel for 7 days (bar = 200 μm), and **(h)** metabolic activity (PrestoBlue) over time. Data are presented as mean ± SD with statistical significance indicated by *$P < .05$, **$P < .001$, and ***$P < .0001$, using 1-way ANOVA; n > 3. 3D, 3-dimensional; Au, arbitrary unit; nMFI, normalized mean fluorescent intensity; ; Tc, cytotoxic T; Th1, T helper 1.

significantly increased granzyme B abundance ($P < .001$) compared with both naïve (IL-2 alone) or activated (IL-2 + CD3 and CD28) stimulated CD8+ T cells, confirming their Tc cell status (Figure 1e). Moreover, Tc cells displayed the highest increase in cell number (Figure 1f). When incorporated into collagen hydrogels, both Th1 and Tc cells were evenly distributed within the gel (Figure 1g). The number of Th1-polarized cells was significantly increased in collagen gels compared with that in naïve T-cells either when polarized before addition to the collagen or when within the gel itself (Figure 1h).

Cytokine and chemokine production by tissue-engineered OMEs upon stimulation with inflammatory (recombinant IFN-γ and TNF-α) or Th1-secreted cytokines
Upon culture with IFN-γ and TNF-α, T-cell polarization medium (PM) alone, or conditioned polarization medium after culture with T cells (ie, PM + Th1), the overall morphology of OMEs in the absence of T-cells was similar to that of native buccal oral mucosa. In each case, the OMEs displayed a stratified squamous epithelium with increasing keratinocyte differentiation toward the apical epithelial surface, with the epithelium attached to a fibroblast-populated connective tissue (Figure 2a), as previously observed (Jennings et al, 2016). Upon stimulation with IFN-γ and TNF-α, to mimic Langerhans cell activation after antigen recognition, the epithelium increased in thickness (368 ± 66 μm) compared with that of the unstimulated control OMEs (118 ± 21 μm, $P = .017$), indicating hyperproliferation (Figure 2a). In contrast, the epithelial thickness of OMEs cultured in PM alone or PM + Th1 showed no effect on epithelial thickness (193 ± 75 μm and 232 ± 74 μm, respectively). No epithelial apoptosis or basement membrane disruption was observed in any of the conditions (Figure 2a).

Upon stimulation with IFN-γ and TNF-α, OMEs in the absence of T-cells showed increased secretion of several cytokines and chemokines, when assessed by protein array, particularly in response to IFN-γ and TNF-α or PM + Th1 (Figure 2b). Array analysis showed that secretion of monocyte-specific chemokines CCL7 (monocyte chemotactic protein 3) and CCL8 (monocyte chemotactic protein 2) were increased 26- and 8-fold, respectively, in the IFN-γ— and TNF-α—stimulated OMEs, with an 11- and 5-fold increase, respectively, in the PM + Th1—conditioned medium, compared with those of controls. Secretion of T-cell—specific chemokines CXCL9 (MIG), CXCL10 (IP10), and CCL5 (RANTES) were increased in the IFN-γ— and TNF-α—stimulated OMEs by 3-, 6-, and 9-fold, respectively, and in the PM + Th1—conditioned medium by 3-, 5- and 13-fold, respectively (Figure 2c). CCL4 (MIP-1β), a chemokine that attracts CD4+ T-cells, and CCL1 (I-309), a monocyte chemoattractant, showed an 8- and 4-fold increase, respectively, in the PM + Th1 compared with that in PM-only conditioned medium and were not secreted upon IFN-γ and TNF-α stimulation. Other notable increases in PM + Th1—treated OMEs were IL-13 (72-fold), IL-10 (8-fold), GM-CSF (16-fold), and TNF-β (10-fold) compared with those in the PM alone (Figure 2c). PM + Th1—conditioned medium also contained abundant IFN-γ and TNF-α, confirming their release upon Th1 polarization as previously assessed (Figures 1b and c and 2c).

To validate the array data, CXCL9, CXCL10, and CCL5 were further quantified by ELISA. Production of CXCL9 by OMEs was significantly increased in response to both IFN-γ and TNF-α (2.7 ± 0.2 ng/ml, $P < .001$) and PM + Th1 medium (2.6 ± 0.5 ng/ml, $P < .001$) compared to their respective controls (PM alone: 0.2 ± 0.2 ng/ml, untreated control: 0.1 ± 0.1 ng/ml) (Figure 2d). A similar secretion profile was observed for CXCL10 with significantly elevated levels in both IFN-γ— and TNF-α—treated OMEs (1.7 ± 0.5 ng/ml, $P < .001$) and PM + Th1—conditioned medium (1.7 ± 0.4 ng/ml, $P < .01$) compared with that in PM alone (0.2 ± 0.2 ng/ml) and unstimulated control (0.06 ± 0.05 ng/ml) (Figure 2e). Levels of CCL5 were significantly increased in PM + Th1—treated OMEs (0.3 ± 0.1 ng/ml) ($P < .05$) compared with that in PM alone (0.07 ± 0.02 ng/ml), but no difference was found between IFN-γ— and TNF-α—stimulated and unstimulated control (Figure 2f). Taken together, these data show that cytokine-stimulated OMEs produce several potent T-cell chemokines that are capable of directing T-cell migration toward the epithelium.

Development of a full-thickness tissue-engineered T-cell inflammatory OMEs
To generate a T-cell inflammatory OMEs (denoted as T-cell-OME), OMEs were combined with a Th1- and Tc-populated collagen hydrogel at day 7 culture to form a layer-on-layer culture model (Figure 3a and b and Supplementary Figure S2a—c). The T-cell-OME therefore consists of a stratified squamous epithelium, followed by a fibroblast-populated connective tissue and then a third layer containing a combination of Th1 and Tc cells (Figure 3b). At day 10 culture, T-cell-OMEs were stimulated with topical application of IFN-γ and TNF-α to induce cytokine and chemokine production and analyzed over a 15-day period. By day 12, the oral epithelium began to display signs of keratinocyte basal cell and basement membrane damage with epithelial detachment from the connective tissue in places, although T-cells remained in the lower layer of the model (Figure 3c). At day 16, further epithelium damage and destruction of the basement membrane were evident, and presence of T-cell recruitment at the stratum basale was observed compared with that of OMEs without T-cells (Figure 3c). Tissue destruction gradually progressed overtime until a complete loss of tissue integrity on day 25 (Figure 3c). These events were not observed with OMEs, which displayed complete structural integrity but thinning of the epithelium on day 25 (Figure 3c). On days 20 and 25, the T-cell-OMEs were fragile and difficult to handle owing to loss of tissue integrity; therefore, T-cell-OMEs at days 12—15 best represented disease and were also the most amenable to further analysis.

To confirm the presence of key T-cell—specific chemokines, conditioned media was collected from the models on days 12—25, and levels of CXCL9, CXCL10, and CCL5 were quantified. At all time points examined, levels of CXCL9, CXCL10, and CCL5 were significantly ($P < .001$) increased in the T-cell-OMEs compared with those in the OME alone (Figure 3d—f), indicating the presence of an abundant T-cell chemotactic profile, facilitating T-cell recruitment to the epithelium.
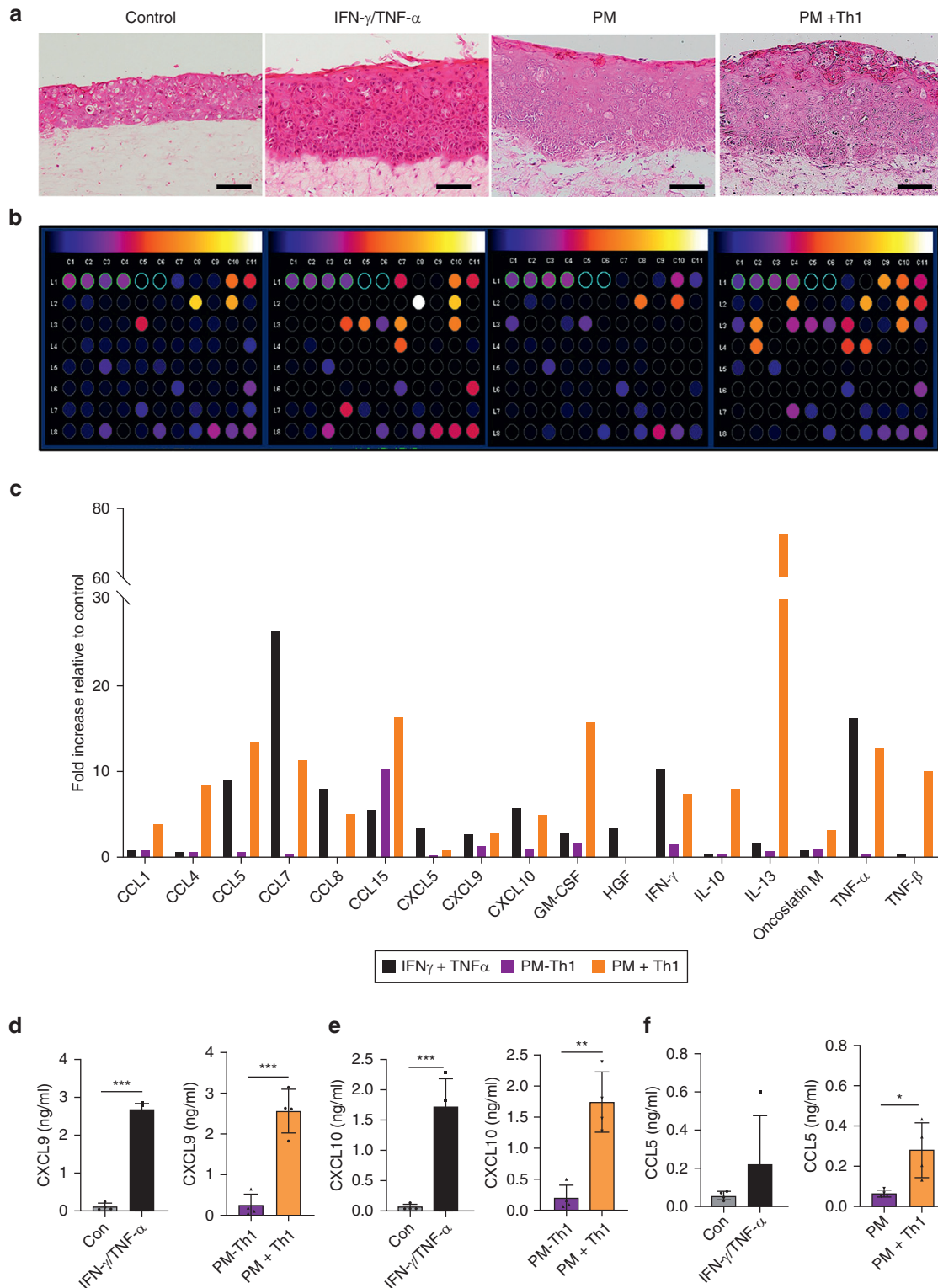
Figure 2. OME inflammatory cytokine secretions after stimulation. (a) Representative H&E histology staining of OMEs cultured for 10 days and either left unstimulated (control), stimulated with IFN-γ and TNF-α, PM, or Th1-conditioned PM (ie, PM +Th1) for 48 hours. Bar =100 μm. **(b)** Secretion of inflammatory cytokines detected using a cytokine array and **(c)** semiquantified using densitometry (n = 2 [only cytokines with >3-fold increases compared with control are shown, full data are presented in supplementary Figure S3]). T-cell chemokines **(d)** CXCL9, **(e)** CXCL10, and **(f)** CCL5 were quantified by ELISA. Data are presented as mean ± SD, with statistical significance indicated by *P < .05, **P < .001, and ***P < .0001 using a Student's t-test; n = 3. OME, oral mucosal equivalent; PM, polarization media; Th1, T helper 1.
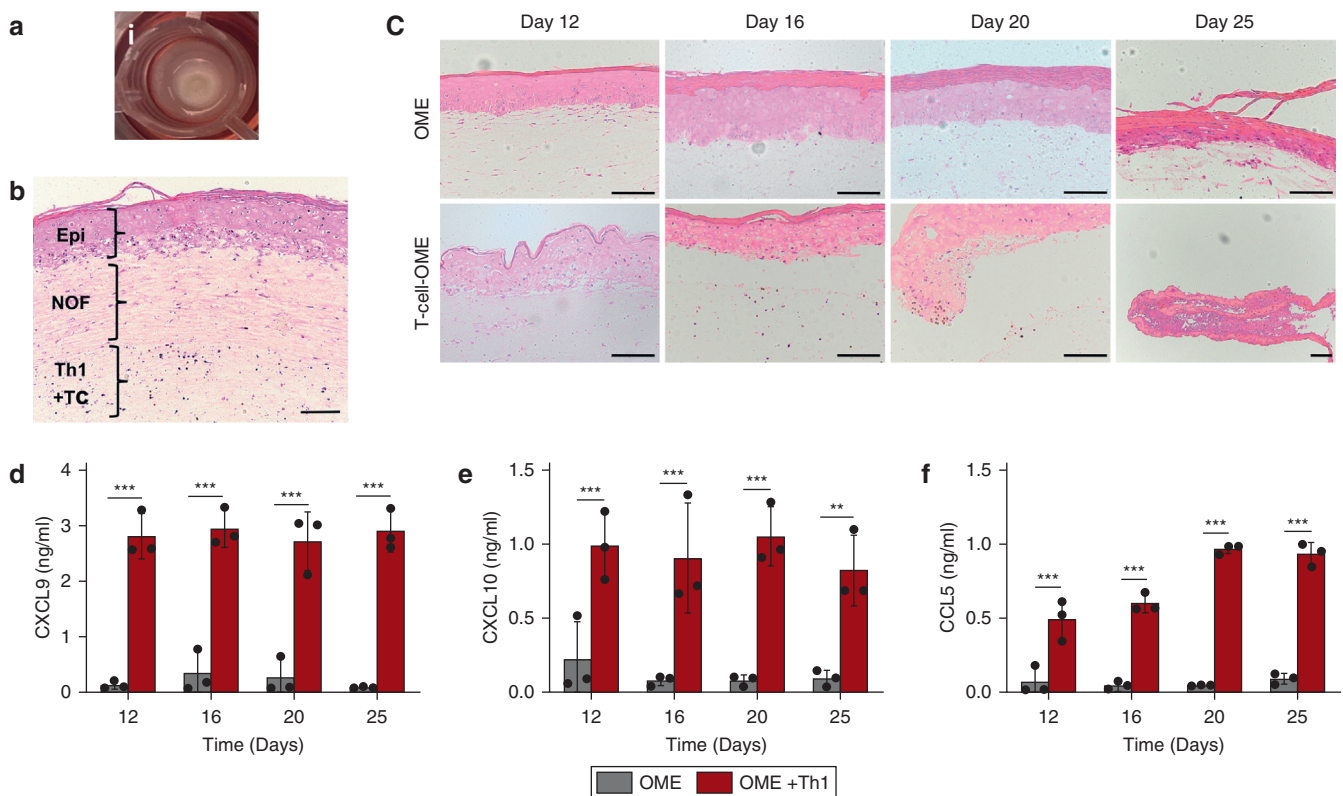
Figure 3. Development of a full-thickness T-cell inflammatory OMEs (denoted as T-cell-OMEs). (a) T-cell-OMEs cultured at an air-to-liquid interface for 12 days were analyzed by histology, with H&E staining showing evidence of an epithelium (denoted as Epi) and a **(b)** NOF-populated connective tissue on top of a dense band of inflammatory T-cells (Th1 +Tc) in the subepithelial compartment. Bar = 100 μm. **(c)** After stimulation with IFN-γ and TNF-α for 48 h, histological analysis revealed evidence of T-cells infiltrating toward the epithelium and epithelial destruction overtime. Bar = 100 μm. Key T-cell–specific chemokines **(d)** CXCL9, **(e)** CXCL10, and **(f)** CCL5 (quantified by ELISA) were increased in the T-cell-OME compared with those in the OMEs alone at all time points examined. Data are presented as mean ± SD, with statistical significance indicated by **P < .001 and ***P < .0001 using Student's t-test at each time point; n = 3. h, hour; NOF, normal oral fibroblast; OME, oral mucosal equivalent; Tc, cytotoxic T; Th1, T helper 1.

Immunohistochemical validation of the T-cell-OMEs against human OLP biopsy tissue

The main histological features of OLP are high T-cell numbers in the connective tissue immediately adjacent to the epithelium as well as within the stratum basale, basal keratinocyte apoptosis, and basement membrane liquefaction. Histological analysis of T-cell-OMEs at day 12 displayed all these classical features (Figure 4a) and was comparable with histological sections from patients with OLP (Figure 4b).

Immunohistochemical staining was performed on T-cell-OMEs to validate the model against OLP patient biopsies. T-cell-OMEs stained immunopositive for CD4+ Th1 and CD8+ Tc cell surface markers, localizing these cells to areas adjacent to and within areas of epithelial destruction, indicating that many Th1 and Tc cells had migrated toward and were recruited to the epithelium (Figure 4c). Indeed, the pattern of Th1 and Tc cell recruitment that was observed in the T-cell-OMEs was similar to that observed in OLP (Figure 4c). Immunostaining for laminin-5, a glycoprotein constituent of the basement membrane, revealed a continuous immunopositive band at the basement membrane zone and the intercellular spaces in the stratum basale in OMEs (Figure 4c). In contrast, laminin-5 immunostaining was more diffuse in the T-cell-OMEs, revealing thin irregularly scattered laminin-5 filaments corresponding to a fragmented,

incoherent basement membrane, reflecting the loss of basement membrane integrity as the basal keratinocytes detach from the connective tissue in the disease state (Figure 4c). Similar laminin-5 staining was observed in the biopsies of patients with OLP in areas of epithelial–connective tissue damage, indicating basement membrane liquefaction (Figure 4c). The presence of cleaved caspase-3, a marker for apoptosis, was not observed in OMEs. In contrast, abundant cleaved caspase-3 was detected in the basal and suprabasal areas of the epithelium as well as in the subepithelial T-cell inflammatory infiltrate in both T-cell-OMEs and OLP biopsies (Figure 4c).

Anti-inflammatory drugs reduce T-cell–mediated inflammation in a T-cell-OMEs

Having established an in vitro model of inflammatory T-cell–mediated oral disease, we next tested whether this model could be used as a test platform to examine drug efficacy. In this study, we used secretion of the important OLP T-cell chemokine, CCL5, as a marker to screen for drug performance against anti-inflammatory drugs currently used to treat other conditions. Topical treatment of T-cell-OMEs with the JAK-1 and 2 inhibitor ruxolitinib (Lin et al, 2009) (P < .01); the K$_{Ca}$3.1 channel inhibitor, NS6180 (Strøbæk et al, 2013) (P < .05); and the potent corticosteroid, clobetasol-

ARTICLE IN PRESS

A El-Howati et al.
In Vitro Modelling of T-Cell Mediated Inflammatory Disease

Figure 4. Immunohistochemical validation of the T-cell inflammatory OME (T-cell-OME) against human OLP biopsy tissue. H&E staining showing T-cells infiltrating the epithelium and basement membrane destruction in **(a)** day-12 T-cell-OMEs compared with that in **(b)** a human OLP biopsy. Bar = 200 μm. **(c)** Immunohistochemical staining for the presence of CD4+ Th1 and CD8+ Tc T-cells and positive staining of laminin-5 revealing the basement membrane and apoptosis (cleaved caspase-3–positive) staining in OME, T-cell-OME, and OLP biopsies. Bar = 100 μm. OLP, oral lichen planus; OME, oral mucosal equivalent; Tc, cytotoxic T; Th1, T helper 1.
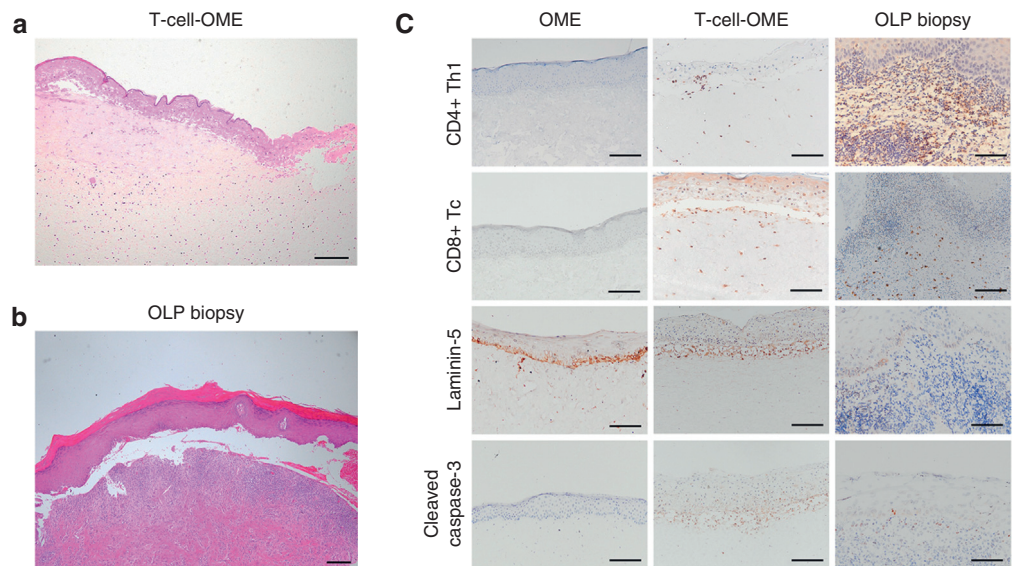
17-propionate ($P < .01$), all significantly inhibited the release of CCL5 by T-cell-OMEs compared with that in untreated controls (Figure 5). CCL5 levels were reduced upon treatment with decernotinib, a JAK-3 inhibitor, and roflumilast, a phosphodiesterase-4 inhibitor, but not significantly different from that of the controls (Figure 5).

We next examined the mode of mucosal drug delivery by comparing clobetasol-17-propionate delivered in solution with that delivered through a clobetasol-containing mucoadhesive polymer membrane (Figure 6a) (Colley et al, 2018; Said et al, 2021). Untreated T-cell-OMEs or those treated with a placebo mucoadhesive membrane displayed significant epithelial damage associated with high levels of
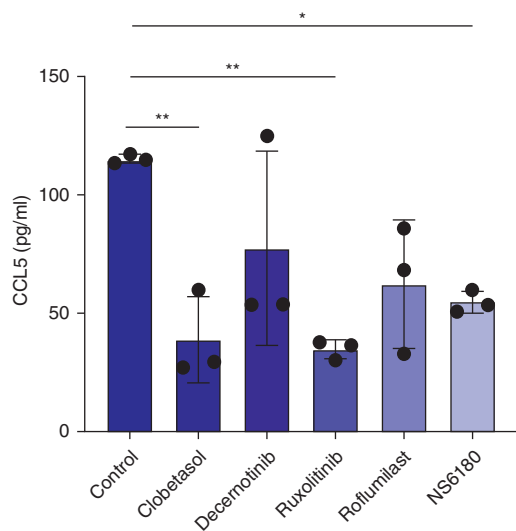
cleaved caspase-3 immunopositive cells at the epithelial–connective tissue interface along with disrupted laminin-5 staining and epithelial separation from the connective tissue (Figure 6b). In contrast, T-cell-OMEs treated with either clobetasol-17-propionate in solution or released from a mucoadhesive membrane displayed an intact epithelium with few signs of tissue damage; immunohistochemical analysis showed sparse cleaved caspase-3 staining. Laminin-5 immunostaining was continuous and well-defined in the basement membrane zone, and the epithelium was attached to the connective tissue. These data indicate inhibition of the deleterious T-cell–mediated inflammatory effects observed in nonmedicated OMEs. Moreover, both solution and mucoadhesive membrane forms of clobetasol treatment significantly reduced the secretion of key T-cell chemokines, including CCL5 ($P < .05$) (Figure 6c), CXCL9 ($P < .001$) (Figure 6d), and CXCL10 ($P < .05$) (Figure 6e). Interestingly, the placebo mucoadhesive patch also reduced the levels of these chemokines in the conditioned medium (Figure 6c–e), although it did not prevent T-cell–mediated tissue damage (Figure 6b).

DISCUSSION

A lack of preclinical experimental models is currently hampering the development and testing of therapeutic agents as well as new forms of drug delivery for the treatment of several oral mucosal inflammatory diseases, where tissue destruction and disease are propagated by a dysregulated immune response. There are no animal models that represent conditions such as OLP, oral aphthous ulcers, or oral ulcers caused by Behçet's disease. Moreover, the oral mucosa of rodents is structurally very different from that of humans, making translation of any experimental in vivo data problematic (Sa et al, 2016). Therefore, development of tissue-engineered human OMEs that incorporate immune cells is required to fill this gap in preclinical models.

When developing complex tissue-engineered constructs, it is of paramount importance to use the most appropriate cell types and replicate the structural and environmental

Figure 5. Anti-inflammatory drug screen in T-cell inflammatory OME (T-cell-OME). Clobetasol-17-propionate, decernotinib, ruxolitinib, roflumilast, or NS6180 was topically applied to T-cell-OMEs, and the levels of secreted CCL5 were determined by ELISA and compared with those of untreated controls. Data are presented as mean ± SD, with statistical significance indicated by $*P < .05$ and $**P < .001$ using a 1-way ANOVA; n = 3. OME, oral mucosal equivalent.
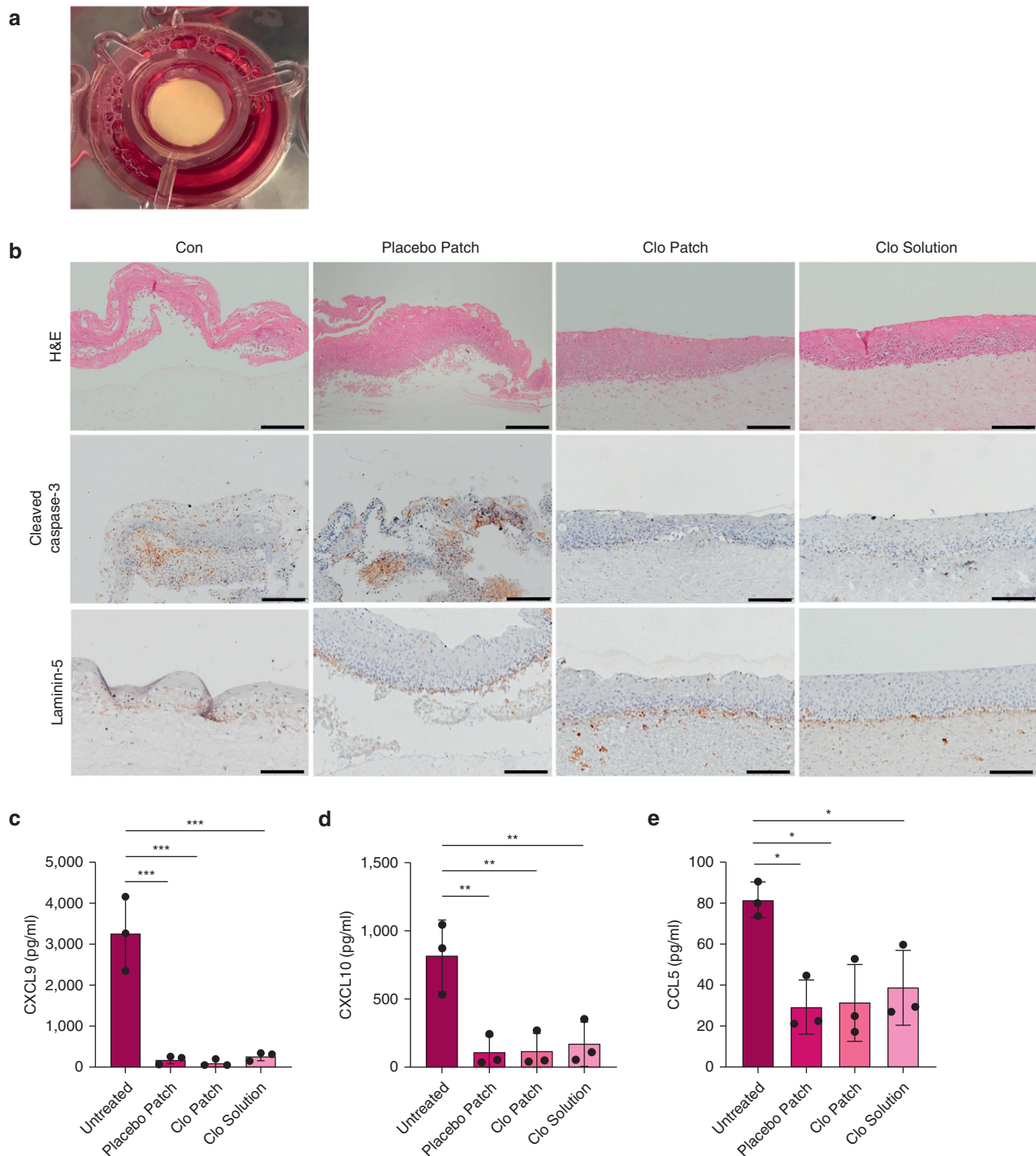
Figure 6. Clobetasol-17-proprionate delivered topically through a mucoadhesive patch reduces T-cell−mediated inflammation in a T-cell inflammatory OME (T-cell-OME). (a) Clobetasol-17-propionate was delivered topically to T-cell-OMEs through a clobetasol-containing mucoadhesive patch (denoted as Clo-Patch) or in solution (denoted as Clo-Solution) and compared with that of untreated T-cell-OME or those treated with a nonmedicated mucoadhesive patch (placebo). Histological and immunohistochemical staining showed extensive epithelial damage with separation from the underlying connective tissue, high levels of cleaved caspase-3−immunopositive cells, and disrupted laminin-5 staining in the untreated T-cell-OME. **(b)** In contrast, T-cell-OME treated with either clobetasol-17-propionate released from a mucoadhesive patch or in solution displayed an intact epithelium with few signs of tissue damage. T-cell−specific chemokines **(c)** CXCL9, **(d)** CXCL10, and **(e)** CCL5 (quantified by ELISA) were reduced in the T-cell-OMEs treated with the placebo, Clo-Solution, and Clo-Patch. Data are presented as mean ± SD, with statistical significance indicated by *P < .05, **P < .001, and ***P < .0001 using a 1-way ANOVA; n = 3. Con, control; OME, oral mucosal equivalent.

conditions that are observed in human tissue. The tissue-engineered human OMEs used in this study have previously been extensively validated against human oral mucosa for structural as well as key cell marker (cytokeratin, ki-67, desmosome, etc) profiles (Jennings et al, 2016; Said et al, 2021). Analysis of ex vivo tissue biopsies of OLP shows

large subepithelial infiltrates of CD4+ Th1 cells and CD8+ Tc cells that are intimately involved in pathogenesis (Jungell et al, 1989; Khan et al, 2003; Matthews et al, 1984), meaning that these specific T-cell phenotypes need to be incorporated into the OMEs in the right location and cell densities and at the right time to replicate the human in vivo situation.

Optimizing T-cell culture and validating their phenotype are crucial when combining these cells to OMEs. In this study, T-cell activation was achieved using anti-CD3 and CD28−coated beads to simulate TCR activation by antigen-presenting cells, which provides a more physiologically relevant stimulus than chemical activation (Martkamchan et al, 2016; Trickett and Kwan, 2003). Incubation of CD4+ T cells with specific cytokines (IL-2, IL-12, IL-18, and anti−IL-4) drives their expansion and polarization into Th1 cells (Amsen et al, 2009) that are validated by the increased abundance of the transcriptional factor T-bet and signal transducer and activator of transcription 4 and secretion of IFN-γ and TNF-α, key Th1 cytokines involved in Th-1−mediated disease pathogenesis (Thieu et al, 2008; Usui et al, 2006). Cytotoxic CD8+ T cells were validated by production of granzyme B (Krähenbühl et al, 1988; Patel et al, 2018).

In OLP, Langerhans cells located in the spinous epithelium acquire and respond to an unknown antigen to initiate the disease process by secretion of proinflammatory factors (principally, IFN-γ and TNF-α) that interact with the oral epithelium, driving the release of more cytokines before they migrate to the locoregional lymph nodes to present antigen and activate T-cells (mimicked by CD3 and CD28 ligation in this study) (El-Howati et al, 2023; Rich and Reade, 1989). This aspect of pathogenesis is difficult to replicate in vitro. Although antigen-presenting cells such as dendritic cells have been incorporated into OMEs previously (Kosten et al, 2016; Schuster et al, 2014), the lack of a known antigen driver in OLP means that their presence can be negated by the addition of recombinant IFN-γ and TNF-α to mimic antigen-induced cell activation (where the option of adding further activated dendritic cell−secreted cytokines may improve imitation). Moreover, upon IFN-γ and TNF-α stimulation, OMEs secreted elevated levels of numerous cytokines and chemokines associated with T-cell recruitment (Ichimura et al, 2006) and an OLP disease profile (Yamamoto and Osaki, 1995; Yamamoto et al, 1994).

The different time scales and media required to culture OMEs and polarize T-cells meant that these had to be cultured separately and then brought together at the required time. Previously, Said et al (2021) added a suspension of phytohaemagglutinin-activated Jurkat cells (a T-cell leukaemia cell line) to the medium under the OME-containing transwell, but this experimental setup does not allow T-cells to enter the collagen connective tissue. In contrast, van den Bogaard et al (2014) applied a suspension of T-cells to the basolateral side of tissue-engineered skin equivalents by lifting the skin equivalent at one edge, adding the T-cells by pipette, and then lowering the models onto the T-cells so that the T-cells were in direct contact with the basolateral side of the collagen. In our hands, this methodology caused T-cells to be forced up between the OMEs and the inner side of the transwell wall, and displacement of the

normal oral fibroblast (NOF)−populated collagen from the transwell filter was frequently observed. We therefore opted to encapsulate the T-cells within a collagen gel and then attach the OMEs onto this gel using a thin layer of collagen as an adhesive, creating a layer-on-layer T-cell containing model (T-cell-OMEs). To our knowledge, this technique has not been previously described. We believe that this type of model permits more controlled addition of T-cells (or any other cell type required) to OMEs, compared with other systems.

Upon coculture, localization of T-cells adjacent to and within the epithelium suggests the establishment of a chemotactic gradient that facilitates the recruitment of Th1 cells from the basolateral collagen layer into the upper OME layer. Cytokine array and ELISA analysis of IFN-γ− and TNF-α−stimulated OMEs suggest that elevated levels of the T-cell−specific chemokines CXCL9 and 10 and CCL5 are likely responsible for the T-cell migration, presumably by binding to their receptors CXCR3 and CCR5, respectively. These data match observations from OLP biopsies where high levels of CXCL9, CXCL10, CXCL11, and CCL5 (Zhao et al, 2002) were detected in the epithelium and lamina propria of patients with OLP (Fang et al, 2019; Ichimura et al, 2006; Little et al, 2003; Zhao et al, 2002), whereas increased levels of CCR5 were detected on T-cells within patients with OLP (Hu et al, 2013). Recently, Shan et al (2019) suggested that CCL5 acts in an autocrine manner to form a positive feedback loop to establish chronicity of OLP. The similarity in T-cell recruitment between the T-cell-OMEs and OLP lesions indicates the possibility of using T-cell-OMEs to dissect the major chemoattractant pathways involved in OLP, thereby identifying possible therapeutic targets.

As well as CD4+ and CD8+ T-cell recruitment, the T-cell-OMEs displayed basal keratinocyte cleaved caspase-3−mediated apoptosis and basement membrane liquefaction as observed by disrupted laminin-5 staining, matching observations seen in OLP biopsies (Dekker et al, 1997; Matthews et al, 1984; Shimizu et al, 1997; Tobón-Arroyave et al, 2004), and are widely recognized as the main pathological features of OLP. Although some intraepithelial CD4+ and CD8+ T cells were observed by immunohistochemistry at day 12, many of these T-cells remained in the subepithelial connective tissue, suggesting that secreted factors released by T-cells in addition to intraepithelial-located T-cells may be important in causing tissue damage. It could be hypothesized that in OLP, the increased secretion of soluble mediators such as TNF-α by Th1 cells within the connective tissue causes T-cell−mediated basal cell apoptosis through the activation of death receptors (eg, TNFR1 [Khan et al, 2003]) in a cleaved caspase-3−dependent manner (Jin and El-Deiry, 2006). Intraepithelial CD8+ T-cells may further perpetuate this by granzyme B/perforin (Santoro et al, 2004) or FasL and FasR-mediated apoptosis (Neppelberg et al, 2001). Moreover, Th1 cells may also release matrix metalloproteinases that are capable of degrading basement membrane proteins such as laminin without the need for intimate cell−basement membrane contact (Oviedo-Orta et al, 2008).

Although the T-cell-OME was stimulated only once on day 10, the tissue damage progressed gradually over time, suggesting establishment of cyclic inflammatory events that

eventually destroyed the OME tissue structure by day 25. This progressive phenotype is in line with natural OLP progression where in many instances, there is complete loss of epithelium, giving raise to ulceration. However, this is not always the case, and many lesions remain at the less aggressive reticular stage. Further advancement of the T-cell-OMEs may involve adding different ratios of Th1 and CD8 Tc cells or inclusion of other T-cell subsets such as Th17, T helper 9, T helper 22, or regulatory T-cells in particular, because the levels of these T-cells are known to correlate with OLP severity (Tao et al, 2010), and therefore, addition of regulatory T-cells to T-cell-OMEs may dampen down the immune response and reduce the associated tissue damage.

Our study also demonstrates the usefulness of T-cell-OMEs to assess the actions of potentially new treatments or modes of drug delivery. For example, mucoadhesive patch-delivered clobetasol-17-propionate as well drug in solution substantially reduced cytokine levels and all markers of T-cell—mediated damage, confirming the efficacy of mucoadhesive patch-based drug delivery observed in preclinical and clinical trials (Brennan et al, 2022; Colley et al, 2018). Interestingly, placebo patch alone also reduced cytokine levels and patient-reported outcome scores, an observation previously shown for these polymer patches where it is thought that nonspecific binding interactions between polymer and some proteins prevent their detection by immunoassay (Brennan et al, 2022; Edmans et al, 2022, 2020). Moreover, use of T-cell-OMEs showed efficacy of the selective JAK1 and 2 inhibitor ruxolitinib. Although not yet Food and Drug Administration approved, there have recently been several case reports on the successful use of JAK inhibitors such as tofacitinib (Damsky et al, 2020), abrocitinib (Solimani et al, 2023), upadacitinib (Balestri et al, 2022; Kooybaran et al, 2021; Slater et al, 2024), and baricitinib (Moussa et al, 2022; Rahman et al, 2024) for the treatment of OLP, confirming the data in our T-cell-OME study and suggesting that these types of therapy taken orally or in patch form are promising treatments for OLP.

In summary, this study describes, to our knowledge, the previously unreported development of a complex tissue-engineered T-cell—mediated oral disease model that displayed many of the key characteristics of OLP. This preclinical in vitro disease model has potential to probe for molecular mechanisms of disease and can be used as a platform to test for novel therapeutics and modes of treatment.

MATERIALS AND METHODS
Unless otherwise indicated, all other reagents were purchased from Sigma-Aldrich. ELISAs were purchased from R&D Systems. Poly(vinylpyrrolidone) (molecular weight of 2000 kDa) and Eudragit RS100 (molecular weight of 38 kDa) were kindly donated by BASF and Evonik Industries AG, respectively.

Cell isolation and culture
FNB6-hTERT immortalized oral keratinocytes (FNB6, Ximbio) were cultured in a flavin- and adenine-enriched medium (FAEM) consisting of high-glucose DMEM and Ham's F12 medium in a 3:1 v/v ratio supplemented with 10% v/v fetal bovine serum, epidermal GF (10 ng/ml), adenine (0.18 mM), insulin (5 μg/ml), transferrin

(5 μg/ml), L-glutamine (2 mM), triiodothyronine (0.2 nM), amphotericin B (0.625 μg/ml), penicillin (100 IU/ml), and streptomycin (100 μg/ml) (Jennings et al, 2016). NOFs were isolated from the buccal mucosal connective tissue of a female aged 24 years with written informed consent (ethical approval reference 09/H1308/66) and cultured in DMEM supplemented with fetal bovine serum (10% v/v), L-glutamine (2 mM), penicillin (100 IU/ml), and streptomycin (100 μg/ml), as previously described (Colley et al, 2011).

PBMCs were isolated from buffy coats as previously described (Murdoch et al, 2007). Briefly, buffy coats obtained from the National Blood Service, United Kingdom (ethical approval reference 012597) were diluted 1:1 in calcium ion— and magnesium ion—free Hank's balanced salt solution and mononuclear cells separated by density-gradient centrifugation using Ficoll Paque Plus (GE Healthcare). CD4+ and CD8+ T-cells were purified from mononuclear cells by negative selection using EasySep Human Naïve CD4+ or CD8+ T-Cell Isolation Kits (StemCell Technologies).

T-cell activation and polarization
Naïve CD4+ T-cells were activated using Dynabeads Human T-Activator CD3 and CD28 (Thermo Fisher Scientific) at a 1:1 cell to Dynabeads ratio in the presence of 30 IU/ml recombinant IL-2 (Peprotech) and cultured for 5 days in Th1 PM consisting of FAEM supplemented with 20 ng/ml human recombinant IL-12 p70 (Peprotech), 20 ng/ml human recombinant IL-18 (R&D Systems), and 2.5 μg/ml anti-human IL-4 antibody (BioLegend). Cytotoxic (Tc) CD8+ T cells were generated by incubating naïve CD8+ T cells with CD3 and CD28 Dynabeads and 30 IU/ml recombinant IL-2 in the presence of CD4+ T cells for 5 days. Proliferation was determined by direct counting using phase-contrast light microscopy.

Construction and stimulation of OMEs
OMEs were constructed as previously described (Jennings et al, 2016). In brief, 2.5×10^5/ml NOFs were mixed with rat tail type I collagen, with 1 ml added to 12-mm cell culture transwell inserts (0.4-μm polyethylene terephthalate, Merck Millipore) and incubated at 37 °C in a humidified atmosphere for 30—60 minutes to gel, after which the hydrogel was submerged in media for 48 hours. FNB6 cells (2.5×10^5) were seeded on the surface of NOF-populated collagen hydrogels and cultured submerged for 72 hours, after which OMEs were raised to an air-to-liquid interface and cultured for a further 7 days. To investigate their cytokine secretion profile, OMEs were incubated for 48 hours with FAEM, supplemented with 1000 IU/ml IFN-γ and 1000 IU/ml TNF-α (to mimic Langerhans cell activation) (Kapsenberg, 2003) or with the conditioned medium obtained after incubation of Th1-polarized T-cells with PM (PM + Th1). OMEs cultured with FAEM or PM alone were used as controls. After 48 hours, conditioned media were collected and stored at −80 °C for further analysis, and OMEs were washed in PBS and fixed in 10% v/v PBS-buffered formalin for histological processing.

Incorporation of T-cells into collagen hydrogels
Naive, CD3 and CD28-activated (activated) or CD3 and CD28-activated then polarized (polarized) Th1 T-cells were mixed with rat tail collagen type I (2×10^6 cells/ml); 0.5 ml was added to 12-mm cell culture inserts and incubated at 37 °C for 30 minutes to gel. Inserts were then submerged and Th1 T-cells cultured in PM, whereas CD3 and CD28-activated T cells were cultured in FAEM. Differences in T-cell number within gels were indirectly assessed using the PrestoBlue metabolic assay (Thermo Fisher Scientific), following the manufacturer's instructions.

Fabrication and treatment of a full-thickness T-cell inflammatory OMEs

To generate an inflammatory T-cell disease model (T-cell-OME), OMEs were constructed but scaled to fit into 24-mm cell culture transwell inserts by adding 2-ml collagen and a cell seeding density of 2.5×10^5 for both NOF and FNB6. After 7 days culture at air-to-liquid interface, OMEs were removed from the insert, cut to fit a 12-mm culture insert with a scalpel, and transferred on to the top of a T-cell–containing hydrogel (previously prepared by adding 1×10^6 Th1 cells and 0.5×10^6 Tc cells to 0.5 ml type I collagen and cultured for 5 days) coated with 100 µl of collagen (3 mg/ml) to facilitate adhesion of the 2 hydrogels (Supplementary Figure S2). T-cell-OMEs were cultured in Th1 PM for 3 days and then topically treated with 1000 IU/ml IFN-γ and 1000 IU/ml TNF-α and incubated further before collection of conditioned media from the basolateral compartment of transwells and tissue fixation at 0, 2, 6, 10, and 15 days. To treat T-cell-OME, 6 hours after cytokine stimulation, models were either incubated for 48 hours with solutions of JAK inhibitors ruxolitinib (300 µM), decernotinib (260 µM), roflumilast (300 µM), or NS6180 (100 µM); clobetasol-17-propionate (20 µg/ml); placebo; or clobetasol-17-propionate–containing mucoadhesive patch (20 µg per patch) fabricated as previously described (Colley et al, 2018; Santocildes-Romero et al, 2017) and cut to fit a 12-mm transwell insert or left untreated as control.

Gene expression and protein secretion analysis

Total RNA was extracted (Monarch Total RNA Miniprep Kit, New England Biolabs) following the manufacturer's instructions and then reverse transcribed to cDNA (High-Capacity RT Kit, Thermo Fisher Scientific), with the amount of RNA used kept consistent within experiments. qPCR was performed with TaqMan gene expression assays using VIC-labeled *β-2-microglobulin* (hs00187842_m1) as a reference control gene alongside FAM-labeled target probes for *TBX21* (Hs00894392_m1), *signal transducer and activator of transcription 1* (Hs01013996_m1), and *signal transducer and activator of transcription 4* (Hs01028017_m1). Expression of the target gene was normalized to the abundance of the control gene transcript, *β-2-microglobulin*. Cytokines were detected in OME-conditioned medium using C-Series Human Cytokine Antibody Array C5 (Ray Biotech), following the manufacturer's instruction, for the semi-quantitative detection of 80 human proteins (Supplementary Figure S3). Densitometry was performed using the array analyzer plug-in for ImageJ software. Secretion of TNF-α, IFN-Υ, CCL5, CXCL9, and CXCL10 in conditioned media was quantified by ELISA.

Histological and immunohistochemical analysis

Formalin-fixed OMEs and T-cell-OMEs were paraffin wax embedded using standard histology procedures. Sections (5 µm) were cut using a Leica RM2235 microtome (Leica Microsystems) mounted on SuperfrostPlus slides (Thermo Fisher Scientific), stained with H&E, mounted in dibutylphthalate polystyrene xylene, and imaged using an Olympus BX51 microscope with CellSens Imaging Software (Olympus GmbH). Sections were immersed in 1% periodic acid for 15 minutes and then with Schiff's reagent for 15 minutes before being counterstained with Harris' hematoxylin. For immunohistochemistry, sections were dewaxed, dehydrated, and then incubated for 20 minutes in 3% hydrogen peroxide in methanol to neutralize endogenous peroxidases. Antigen retrieval was achieved using Tris and EDTA buffer (pH 9) or 0.01 M citrate buffer (pH 6) at high temperature. After blocking with normal goat serum for 30 minutes, sections were incubated with primary antibodies—monoclonal rabbit anti-human CD4 (SP35, 1:50, Thermo Fisher Scientific), monoclonal mouse anti-human CD8 (C8/144B, 1:25, Bethyl Laboratories), monoclonal mouse anti-human vimentin (RV202, 1:25, Santa Cruz Biotechnology), monoclonal mouse anti-human laminin-5 (γ2 chain) (D4B5, 1:100, Merck), polyclonal rabbit anti-human cleaved caspase-3 (Asp175, 1:100, Cell Signaling Technologies), anti-rabbit IgG isotype control (7074S, 1:1000, Cell Signaling Technologies), or anti-mouse IgG isotype control (DAK-GO1, 1:200, Agilent)—for 16 hours at 4 °C. Secondary antibody and avidin–biotin complex (Vectastain Elite ABC kit, Vector Laboratories) were used in accordance with the manufacturer's instructions. Finally, 3′-diaminobenzidine tetrahydrochloride (Vector Laboratories) was used to visualize peroxidase activity and the sections counterstained with Harris's hematoxylin.

Flow cytometry

For surface marker staining, 1×10^6 cells were resuspended in 95 µl FACS buffer (PBS with 0.1% BSA and 2 mM EDTA, pH 7.4) and 5 µl of fluorescent-conjugated antibody: CD4 (allophycocyanin, RPA-T4, eBioscience), CD4 (phycoerythrin, RPA-T4, eBioscience), CD8 (allophycocyanin, RPA-T8, Thermo Fischer Scientific), and CD69 (allophycocyanin, FN50, Thermo Fisher Scientific). Samples were incubated for 30 minutes on ice, protected from light, before washing with 1 ml FACS buffer. The LIVE/DEAD fixable blue stain (Thermo Fisher Scientific) was used to exclude dead cells from the analysis. Nuclear and intracellular target staining was performed using antibodies against T-bet transcription factor, a key regulator of Th1 polarization (phycoerythrin-Cyanin7, 4B10, eBioscience), and granzyme B, a protease secreted by CD8+ Tc cells (Alexa Fluor 700, GB11, BD Bioscience), in conjugation with fixation and permeabilization buffers (eBioscience), following the manufacturer's instructions. Samples were washed and fixed in 4% formalin for 15 minutes and resuspended in a 300 µl FACS buffer. Unstained cells were used to exclude background fluorescence, and a relevant IgG isotype was used to exclude nonspecific staining. For multichromatic staining, the ABC Total Antibody Compensation Bead Kit and the ArC Amine Reactive Compensation Bead Kit (Life Technologies) were used to compensate for spectral overlap, and fluorescence minus one samples were used to adjust gating. Flow cytometry was performed using an LSRII (BD Biosciences) and analyzed using FlowJo software, version 10.7 (BD Biosciences).

Data analysis

All data and statistical analyses were performed using GraphPad Prism 10.0 software (GraphPad Software). Unless otherwise stated, data are presented as mean ± SD of at least 3 independent experiments where each experiments used a separate buffy coat and T-cell isolation. Unpaired Student's *t*-test or 1-way ANOVA with Tukey's posthoc test was used for pairwise or groupwise comparisons, respectively, and results were considered statistically significant if $P < .05$.

DATA AVAILABILITY STATEMENT

No large datasets were generated in this study. Data are available upon request.

ORCIDs

Asma El-Howati: http://orcid.org/0000-0002-4263-6846
Jake G. Edmans: http://orcid.org/0000-0002-4539-9145
Martin E. Santocildes-Romero: http://orcid.org/0000-0003-3805-3055
Craig Murdoch: http://orcid.org/0000-0001-9724-122X
Helen E. Colley: http://orcid.org/0000-0003-0053-7468

AUTHOR CONTRIBUTIONS

Conceptualization: HEC, CM; Methodology: AE-H, JGE, CM, HEC; Investigation: AE-H, JGE; Formal Analysis: AE-H, JGE; Validation: AE-H; Visualization: AE-H, HEC, CM; Resources: MES-R, LSM; Funding Acquisition: HEC; Project Administration: HEC; Supervision: CM, HEC; Writing − Original Draft Preparation: AE-H; Writing − Review and Editing: JGE, MES-R, LSM, CM, HEC

SUPPLEMENTARY MATERIAL

Supplementary material is linked to the online version of the paper at www.jidonline.org, and at https://doi.org/10.1016/j.jid.2024.07.038.

REFERENCES

Amsen D, Spilianakis CG, Flavell RA. How are T(H)1 and T(H)2 effector cells made? Curr Opin Immunol 2009;21:153−60.

Balestri R, Bortolotti R, Rech G, Girardelli CR, Zorzi MG, Magnano M. Treatment of oral erosive Lichen Planus With upadacitinib. JAMA Dermatol 2022;158:457−8.

Bao K, Papadimitropoulos A, Akgül B, Belibasakis GN, Bostanci N. Establishment of an oral infection model resembling the periodontal pocket in a perfusion bioreactor system. Virulence 2015;6:265−73.

Björnfot Holmström S, Clark R, Zwicker S, Bureik D, Kvedaraite E, Bernasconi E, et al. Gingival tissue inflammation promotes increased matrix metalloproteinase-12 production by CD200R^low monocyte-derived cells in periodontitis. J Immunol 2017;199:4023−35.

Brennan MT, Madsen LS, Saunders DP, Napenas JJ, McCreary C, Ni Riordain R, et al. Efficacy and safety of a novel mucoadhesive clobetasol patch for treatment of erosive oral lichen planus: a phase 2 randomized clinical trial. J Oral Pathol Med 2022;51:86−97.

Carrozzo M, Porter S, Mercadante V, Fedele S. Oral lichen planus: a disease or a spectrum of tissue reactions? Types, causes, diagnostic algorhythms, prognosis, management strategies. Periodontol 2000 2019;80:105−25.

Colley HE, Hearnden V, Jones AV, Weinreb PH, Violette SM, Macneil S, et al. Development of tissue-engineered models of oral dysplasia and early invasive oral squamous cell carcinoma. Br J Cancer 2011;105:1582−92.

Colley HE, Said Z, Santocildes-Romero ME, Baker SR, D'Apice K, Hansen J, et al. Pre-clinical evaluation of novel mucoadhesive bilayer patches for local delivery of clobetasol-17-propionate to the oral mucosa. Biomaterials 2018;178:134−46.

Damsky W, Wang A, Olamiju B, Peterson D, Galan A, King B. Treatment of severe lichen planus with the JAK inhibitor tofacitinib. J Allergy Clin Immunol 2020;145:1708−17010.e2.

Danso MO, van Drongelen V, Mulder A, van Esch J, Scott H, van Smeden J, et al. TNF-alpha and Th2 cytokines induce atopic dermatitis-like features on epidermal differentiation proteins and stratum corneum lipids in human skin equivalents. J Invest Dermatol 2014;134:1941−50.

DeAngelis LM, Cirillo N, McCullough MJ. The immunopathogenesis of oral lichen planus-Is there a role for mucosal associated invariant T cells? J Oral Pathol Med 2019;48:552−9.

Dekker NP, Lozada-Nur F, Lagenaur LA, MacPhail LA, Bloom CY, Regezi JA. Apoptosis-associated markers in oral lichen planus. J Oral Pathol Med 1997;26:170−5.

Edmans JG, Murdoch C, Santocildes-Romero ME, Hatton PV, Colley HE, Spain SG. Incorporation of lysozyme into a mucoadhesive electrospun patch for rapid protein delivery to the oral mucosa. Mater Sci Eng C Mater Biol Appl 2020;112:110917.

Edmans JG, Ollington B, Colley HE, Santocildes-Romero ME, Siim Madsen L, Hatton PV, et al. Electrospun patch delivery of anti-TNFalpha F(ab) for the treatment of inflammatory oral mucosal disease. J Control Release 2022;350:146−57.

El-Howati A, Thornhill MH, Colley HE, Murdoch C. Immune mechanisms in oral lichen planus. Oral Dis 2023;29:1400−15.

Engelhart K, El Hindi T, Biesalski HK, Pfitzner I. In vitro reproduction of clinical hallmarks of eczematous dermatitis in organotypic skin models. Arch Dermatol Res 2005;297:1−9.

Fang J, Wang C, Shen C, Shan J, Wang X, Liu L, et al. The expression of CXCL10/CXCR3 and effect of the axis on the function of T lymphocyte involved in oral Lichen Planus. Inflammation 2019;42:799−810.

González-Moles MÁ, Warnakulasuriya S, González-Ruiz I, González-Ruiz L, Ayén Á, Lenouvel D, et al. Worldwide prevalence of oral lichen planus: a systematic review and meta-analysis. Oral Dis 2021;27:813−28.

Hu JY, Zhang J, Cui JL, Liang XY, Lu R, Du GF, et al. Increasing CCL5/CCR5 on CD4+ T cells in peripheral blood of oral lichen planus. Cytokine 2013;62:141−5.

Ichimura M, Hiratsuka K, Ogura N, Utsunomiya T, Sakamaki H, Kondoh T, et al. Expression profile of chemokines and chemokine receptors in epithelial cell layers of oral lichen planus. J Oral Pathol Med 2006;35:167−74.

Jang HJ, Lee JB, Yoon JK. Advanced in vitro three-dimensional skin models of atopic dermatitis. Tissue Eng Regen Med 2023;20:539−52.

Jennings LR, Colley HE, Ong J, Panagakos F, Masters JG, Trivedi HM, et al. Development and characterization of in vitro human oral mucosal equivalents derived from immortalized oral keratinocytes. Tissue Eng Part C Methods 2016;22:1108−17.

Jin Z, El-Deiry WS. Distinct signaling pathways in TRAIL- versus tumor necrosis factor-induced apoptosis. Mol Cell Biol 2006;26:8136−48.

Jungell P, Konttinen YT, Nortamo P, Malmström M. Immunoelectron microscopic study of distribution of T cell subsets in oral lichen planus. Scand J Dent Res 1989;97:361−7.

Kapsenberg ML. Dendritic-cell control of pathogen-driven T-cell polarization. Nat Rev Immunol 2003;3:984−93.

Khan A, Farah CS, Savage NW, Walsh LJ, Harbrow DJ, Sugerman PB. Th1 cytokines in oral lichen planus. J Oral Pathol Med 2003;32:77−83.

Klausner M, Handa Y, Aizawa S. In vitro three-dimensional organotypic culture models of the oral mucosa. In Vitro Cell Dev Biol Anim 2021;57:148−59.

Kooybaran NR, Petzold G, Ströbel P, Schön MP, Mössner R. Alleviation of erosive oral and esophageal lichen planus by the JAK1 inhibitor upadacitinib. J Dtsch Dermatol Ges 2021;19:1778−80.

Kosten IJ, Spiekstra SW, de Gruijl TD, Gibbs S. MUTZ-3 Langerhans cell maturation and CXCL12 independent migration in reconstructed human gingiva. ALTEX 2016;33:423−34.

Krähenbühl O, Rey C, Jenne D, Lanzavecchia A, Groscurth P, Carrel S, et al. Characterization of granzymes A and B isolated from granules of cloned human cytotoxic T lymphocytes. J Immunol 1988;141:3471−7.

Lin Q, Meloni D, Pan Y, Xia M, Rodgers J, Shepard S, et al. Enantioselective synthesis of Janus kinase inhibitor INCB018424 via an organocatalytic aza-Michael reaction. Org Lett 2009;11:1999−2002.

Lira-Junior R, Holmström SB, Clark R, Zwicker S, Majster M, Johannsen G, et al. S100A12 expression is modulated during monocyte differentiation and reflects periodontitis severity. Front Immunol 2020;11:86.

Little MC, Griffiths CE, Watson RE, Pemberton MN, Thornhill MH. Oral mucosal keratinocytes express RANTES and ICAM-1, but not interleukin-8, in oral lichen planus and oral lichenoid reactions induced by amalgam fillings. Clin Exp Dermatol 2003;28:64−9.

Lorthois I, Simard M, Morin S, Pouliot R. Infiltration of T cells into a three-dimensional psoriatic skin model mimics pathological key features. Int J Mol Sci 2019;20:1670.

Martkamchan S, Onlamoon N, Wang S, Pattanapanyasat K, Ammaranond P. The effects of anti-CD3/CD28 coated beads and IL-2 on expanded T cell for immunotherapy. Adv Clin Exp Med 2016;25:821−8.

Matthews JB, Scully CM, Potts AJ. Oral lichen planus: an immunoperoxidase study using monoclonal antibodies to lymphocyte subsets. Br J Dermatol 1984;111:587−95.

Moussa A, Colla T, Morrison B, Sinclair R. Effective treatment of oral lichen planus with the JAK inhibitor baricitinib. Australas J Dermatol 2022;63: 276−7.

Murdoch C, Tazzyman S, Webster S, Lewis CE. Expression of Tie-2 by human monocytes and their responses to angiopoietin-2. J Immunol 2007;178: 7405−11.

Neppelberg E, Johannessen AC, Jonsson R. Apoptosis in oral lichen planus. Eur J Oral Sci 2001;109:361−4.

Ollington B, Colley HE, Murdoch C. Immunoresponsive tissue-engineered oral mucosal equivalents containing macrophages. Tissue Eng Part C Methods 2021;27:462−71.

Oviedo-Orta E, Bermudez-Fajardo A, Karanam S, Benbow U, Newby AC. Comparison of MMP-2 and MMP-9 secretion from T helper 0, 1 and 2 lymphocytes alone and in coculture with macrophages. Immunology 2008;124:42−50.

Patel T, Cunningham A, Holland M, Daley J, Lazo S, Hodi FS, et al. Development of an 8-color antibody panel for functional phenotyping of human CD8+ cytotoxic T cells from peripheral blood mononuclear cells. Cytotechnology 2018;70:1−11.

Rahman SM, Memon N, Ahmed F, Rahman N, Haque A. JAK inhibitor baricitinib in the treatment of oral Lichen Planus: a case report. J Dermatol Res 2024;5:1−4.

Rich AM, Reade PC. A quantitative assessment of Langerhans cells in oral mucosal lichen planus and leukoplakia. Br J Dermatol 1989;120:223−8.

Sa G, Xiong X, Wu T, Yang J, He S, Zhao Y. Histological features of oral epithelium in seven animal species: as a reference for selecting animal models. Eur J Pharm Sci 2016;81:10−7.

Said Z, Murdoch C, Hansen J, Siim Madsen L, Colley HE. Corticosteroid delivery using oral mucosa equivalents for the treatment of inflammatory mucosal diseases. Eur J Oral Sci 2021;129:e12761.

Santocildes-Romero ME, Hadley L, Clitherow KH, Hansen J, Murdoch C, Colley HE, et al. Fabrication of electrospun mucoadhesive membranes for therapeutic applications in oral medicine. ACS Appl Mater Interfaces 2017;9:11557−67.

Santoro A, Majorana A, Bardellini E, Gentili F, Festa S, Sapelli P, et al. Cytotoxic molecule expression and epithelial cell apoptosis in oral and cutaneous lichen planus. Am J Clin Pathol 2004;121:758−64.

Schuster C, Mildner M, Mairhofer M, Bauer W, Fiala C, Prior M, et al. Human embryonic epidermis contains a diverse Langerhans cell precursor pool. Development 2014;141:807−15.

Shan J, Li S, Wang C, Liu L, Wang X, Zhu D, et al. Expression and biological functions of the CCL5-CCR5 axis in oral lichen planus. Exp Dermatol 2019;28:816−21.

Shimizu M, Higaki Y, Higaki M, Kawashima M. The role of granzyme B-expressing CD8-positive T cells in apoptosis of keratinocytes in lichen planus. Arch Dermatol Res 1997;289:527−32.

Slater K, Halash K, Kartono F. Oral Lichen Planus successfully treated with upadacitinib. J Drugs Dermatol 2024;23:e104−6.

Solimani F, Mesas-Fernández A, Dilling A, Nast A, Hilke FJ, Ghoreschi FC, et al. The Janus kinase 1 inhibitor abrocitinib for the treatment of oral lichen planus [e-pub ahead of print]. J Eur Acad Dermatol Venereol 2023;37: e996−8.

Strøbæk D, Brown DT, Jenkins DP, Chen YJ, Coleman N, Ando Y, et al. NS6180, a new K(Ca) 3.1 channel inhibitor prevents T-cell activation and inflammation in a rat model of inflammatory bowel disease. Br J Pharmacol 2013;168:432−44.

Tao XA, Xia J, Chen XB, Wang H, Dai YH, Rhodus NL, et al. FOXP3 T regulatory cells in lesions of oral lichen planus correlated with disease activity. Oral Dis 2010;16:76−82.

Thieu VT, Yu Q, Chang HC, Yeh N, Nguyen ET, Sehra S, et al. Signal transducer and activator of transcription 4 is required for the transcription factor T-bet to promote T helper 1 cell-fate determination. Immunity 2008;29: 679−90.

Tobón-Arroyave SI, Villegas-Acosta FA, Ruiz-Restrepo SM, Vieco-Durán B, Restrepo-Misas M, Londoño-López ML. Expression of caspase-3 and structural changes associated with apoptotic cell death of keratinocytes in oral lichen planus. Oral Dis 2004;10:173−8.

Trickett A, Kwan YL. T cell stimulation and expansion using anti-CD3/CD28 beads. J Immunol Methods 2003;275:251−5.

Usui T, Preiss JC, Kanno Y, Yao ZJ, Bream JH, O'Shea JJ, et al. T-bet regulates Th1 responses through essential effects on GATA-3 function rather than on IFNG gene acetylation and transcription. J Exp Med 2006;203:755−66.

van den Bogaard EH, Tjabringa GS, Joosten I, Vonk-Bergers M, van Rijssen E, Tijssen HJ, et al. Crosstalk between keratinocytes and T cells in a 3D microenvironment: a model to study inflammatory skin diseases. J Invest Dermatol 2014;134:719−27.

Xiao L, Okamura H, Kumazawa Y. Three-dimensional inflammatory human tissue equivalents of gingiva. J Vis Exp 2018;134:57157.

Yamamoto T, Osaki T. Characteristic cytokines generated by keratinocytes and mononuclear infiltrates in oral lichen planus. J Invest Dermatol 1995;104: 784−8.

Yamamoto T, Osaki T, Yoneda K, Ueta E. Cytokine production by keratinocytes and mononuclear infiltrates in oral lichen planus. J Oral Pathol Med 1994;23:309−15.

Zhao ZZ, Sugerman PB, Walsh LJ, Savage NW. Expression of RANTES and CCR1 in oral lichen planus and association with mast cell migration. J Oral Pathol Med 2002;31:158−62.
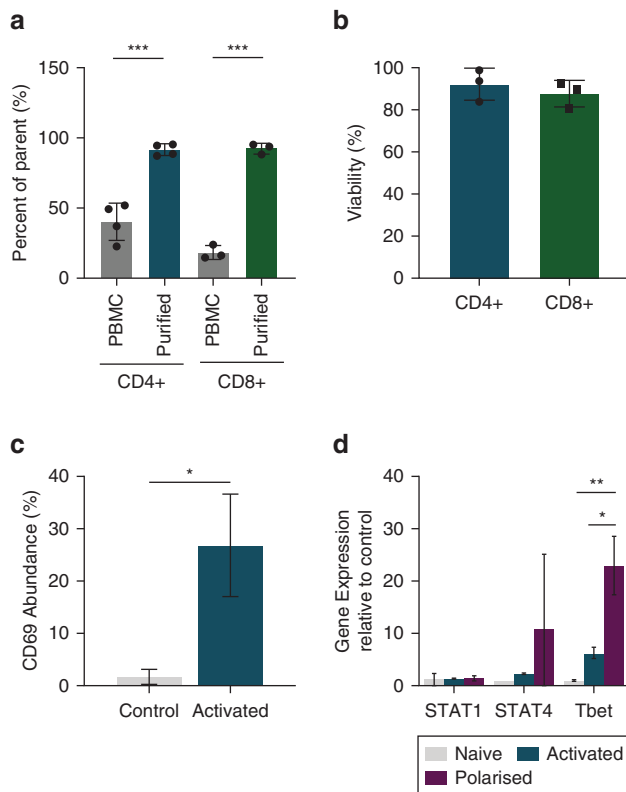
Supplementary Figure S1. CD4+ and CD8+ T-cell isolation purity, viability, activation, and polarized characterization. Peripheral blood mononuclear cells (PBMCs) were isolated through Ficoll density-gradient centrifugation. **(a)** CD4+ and CD8+ T-cells were further purified using EasySep negative selection, and purity was determined as a percentage of the total cell population and **(b)** their viability was determined by live/dead fixable blue stain. **(c)** Percentage of CD4+ T-cell activation after 24 h was determined by increased CD69 levels by flow cytometry. **(d)** Th1 polarization was confirmed by increased gene expression of *STAT4* and *T-bet*. Data are presented as mean ± SD, and statistical analysis was performed using Students's *t*-test. *$P <$ .05, **$P <$ .001, and ***$P <$ .0001; n = 3. h, hour; Th1, T helper 1; STAT4, signal transducer and activator of transcription 4.

A El-Howati et al.
*In Vitro* Modelling of T-Cell Mediated Inflammatory Disease
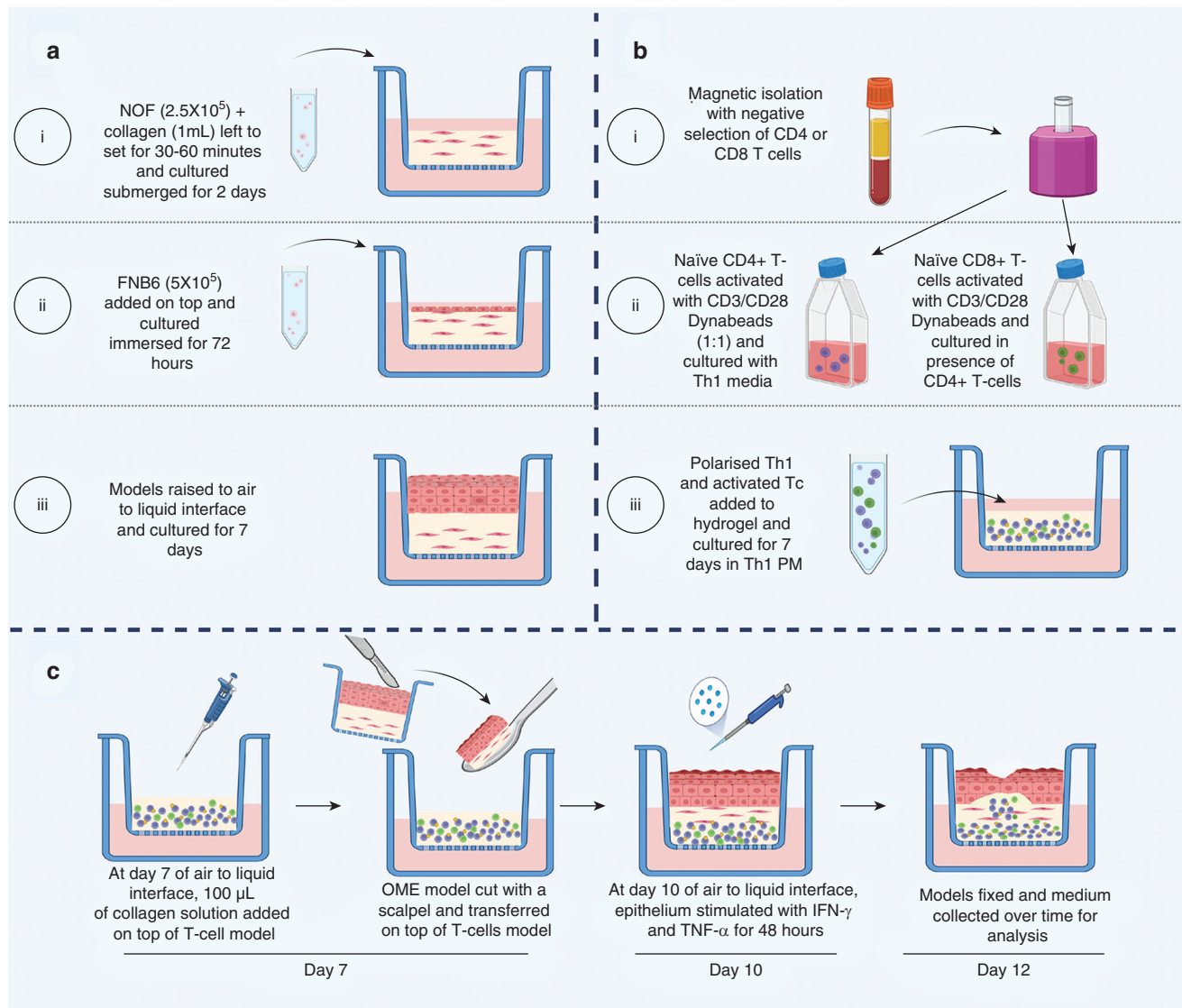
Supplementary Figure S2. Schematic diagram detailing the construction of T-cell OME (denoted as T-cell-OME). (ai−iii) OME were produced by mixing NOF with type I collagen, pipetting 1 mL into transwell inserts and culturing for 2 days. FNB6 oral keratinocytes were seeded on top, cultured submerged for 3 days then at an air-to-liquid interface for 7 days. **(bi−iii)** At the same time, CD4+ and CD8+ T-cells were isolated from peripheral blood mononuclear cells. CD4+ T-cells were polarized to Th1 cells while CD8+ T-cells were activated to Tc T-cells. Both Th1 and Tc T-cells were mixed with type I collagen and incubated for 7 days. **(c)** OME were adhered to the apical surface of the T-cell-containing hydrogen and cultured for a further 3 days at an air-to-liquid interface, At day 10, the epithelium was stimulated with TNF-α and IFN-γ for 48 hours. OME were analysed by histology, immunohistochemistry and cytokine release at day 12 onwards. Image was created with BioRender.com. NOF, normal oral fibroblast; OME, oral mucosal equivalent; PM, polarization media; Tc, cytotoxic T; Th1, T helper 1.

a

	A	B	C	D	E	F	G	H	I	J	K
1	Pos	Pos	Pos	Pos	Neg	Neg	CXCL5	G-CSF	GM-CSF	CXCL1-3	CXCL1
2	I-309	IL-1a	IL-1b	IL-2	IL-3	IL-4	IL-5	IL-6	IL-7	CXCL8	IL-10
3	IL12-p40	IL-13	IL-15	IFN-g	CCL2	CCL8	CCL7	M-CSF	CCL22	CXCL9	CCL4
4	CCL15	CCL5	SCF	CXCL12	CCL17	TGF-b1	TNF-a	TNF-b	EGF	IGF-1	Angiogenin
5	Oncostatin M	TPO	VEGF	PDGF-BB	Leptin	BDNF	CXCL13	CK b 8-1	CCL11	CCL24	CCL26
6	FGF-4	FGF-6	FGF-7	FGF-9	Flt-3 Ligand	CX3CL	CXCL6	GDNF	HGF	IGFBP-1	IGFBP-2
7	IGFBP-3	IGFBP-4	IL-16	CXCL10	LIF	LIGHT	CCL13	MIF	CCL20	CXCL7	NT-3
8	NT-4	Osteopontin	Osteoprotegerin	CCL18	PIGF	TGF-b 2	TGF-b 3	TIMP-1	TIMP-2	Pos	Pos

b
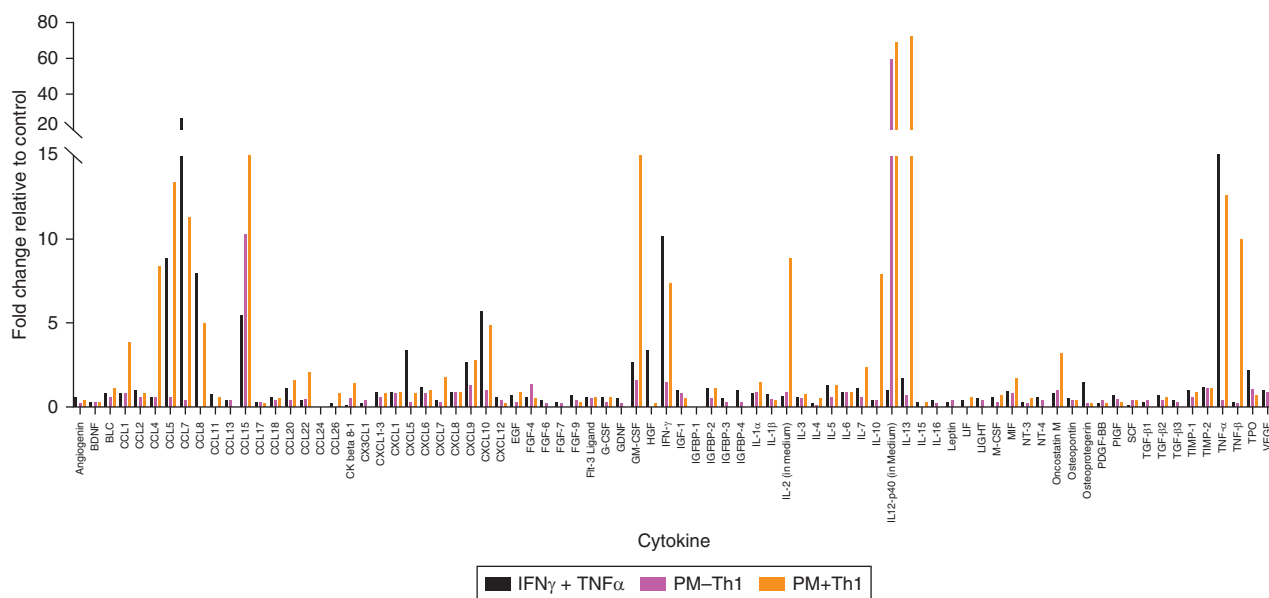
Supplementary Figure S3. Cytokine array key and full analysis. **(a)** Table showing the placement of cytokine detection antibodies on the cytokine array corresponding to the data shown in Figure 2. **(b)** Secretion of inflammatory cytokines detected using a cytokine array and semiquantified using densitometry ($n = 2$).